PHYSICAL REVIEW C **76**, 021001(R) (2007)

Ab initio four-body calculation of n-^{3}He, p-^{3}H, and d-d scattering

A. Deltuva* and A. C. Fonseca
Centro de Física Nuclear da Universidade de Lisboa, P-1649-003 Lisboa, Portugal
(Received 8 March 2007; published 3 August 2007)

Four-body equations in momentum space are solved for neutron-^{3}He, proton-^{3}H, and deuteron-deuteron scattering; all three reactions are coupled. The Coulomb interaction between the protons is included using the screening and renormalization approach as was recently done for proton-deuteron and proton-^{3}He scattering. Realistic potentials are used between nucleon pairs. For the first time fully converged results for the observables pertaining to the six different elastic and transfer reactions are obtained and compared with experimental data.

DOI: 10.1103/PhysRevC.76.021001 PACS number(s): 21.30.−x, 21.45.+v, 24.70.+s, 25.10.+s

Modern studies of nuclear structure are developed by means of *ab initio* calculations of the quantum many-body system using realistic potentials. While at present there is a number of successful *ab initio* structure calculations using Green's function Monte Carlo (GFMC) methods [1,2] and No Core Shell Model [3], *ab initio* studies of nuclear reactions are still limited to a few specific few-nucleon reactions. The difficulties associated with the treatment of the long-range Coulomb interaction restricted, until recently, precise calculations to neutron-deuteron (n-d) elastic scattering and breakup [4] and to proton-deuteron (p-d) [5], n-^{3}H [6], and p-^{3}He [7] elastic scattering at low energy. The situation has now changed because of the work in Ref. [8]. Using the ideas of screening and renormalization [9,10], fully converged results for observables in p-d elastic scattering and breakup were obtained for a wide range of energies and configurations using realistic force models. Other developments have taken place recently using the GFMC approach [11] to calculate the n-^{4}He phase shifts at energies well below the inelastic threshold.

In the present work we attempt to further extend *ab initio* calculations of the four-nucleon ($4N$) system by solving the Alt, Grassberger, and Sandhas (AGS) equations [12] for the n-^{3}He, p-^{3}H, and d-d reactions. This is the most complex scattering calculation that has been attempted so far because all three reactions are coupled and involve both isospin $\mathcal{T} = 0$ and $\mathcal{T} = 1$ states, together with a very small admixture of $\mathcal{T} = 2$ due to the charge dependence of the hadronic and electromagnetic interactions. This work is the continuation of two previous works for n-^{3}H [13] and p-^{3}He [14] where the $4N$ scattering problem was calculated with the same level of accuracy as it already exists for the three-nucleon ($3N$) system. This means that calculations are carried out without approximations on the two-nucleon ($2N$) transition matrix (t matrix) like in Ref. [15] or limitations on the choice of basis functions as in Ref. [16]. Therefore, after partial-wave decomposition, the AGS equations are three-variable integral equations that are solved numerically without any approximations beyond the usual discretization of continuum variables on a finite momentum mesh. Therefore discrepancies with data may be attributed solely to the underlying $2N$ forces or to the lack of $3N$ forces.

*deltuva@cii.fc.ul.pt

The equations we solve are based on the symmetrized four-body AGS equations of Ref. [13]. To include the Coulomb interaction we extend the methodology of Refs. [8] and [14] to all elastic and transfer reactions of the $4N$ system. We add to the nuclear pp potential the screened Coulomb one $w_R(r) = w(r)\exp(-(r/R)^n)$ that in configuration space approximates well the pure Coulomb potential $w(r)$ for $r < R$ and simultaneously vanishes rapidly for $r > R$, providing a comparatively fast convergence of the partial-wave expansion. The optimal smoothness of the screening is ensured by the values $4 \leqslant n \leqslant 8$. The screening radius R must be considerably larger than the range of the strong interaction but from the point of view of scattering theory w_R is still of short range. Therefore, the equations of Ref. [13] become R dependent. The transition operators $\mathcal{U}^{\alpha\beta}_{(R)}$, where $\alpha(\beta) = 1$ and 2 corresponds to initial/final $1 + 3$ and $2 + 2$ two-cluster states, respectively, satisfy the symmetrized AGS equations

$$\mathcal{U}^{11}_{(R)} = -(G_0 t^{(R)} G_0)^{-1} P_{34} - P_{34} U^1_{(R)} G_0 t^{(R)} G_0 \mathcal{U}^{11}_{(R)} + U^2_{(R)} G_0 t^{(R)} G_0 \mathcal{U}^{21}_{(R)}, \tag{1a}$$

$$\mathcal{U}^{21}_{(R)} = (G_0 t^{(R)} G_0)^{-1}(1 - P_{34}) + (1 - P_{34}) U^1_{(R)} G_0 t^{(R)} G_0 \mathcal{U}^{11}_{(R)}, \tag{1b}$$

for $1 + 3$ as the initial state, and

$$\mathcal{U}^{12}_{(R)} = (G_0 t^{(R)} G_0)^{-1} - P_{34} U^1_{(R)} G_0 t^{(R)} G_0 \mathcal{U}^{12}_{(R)} + U^2_{(R)} G_0 t^{(R)} G_0 \mathcal{U}^{22}_{(R)}, \tag{2a}$$

$$\mathcal{U}^{22}_{(R)} = (1 - P_{34}) U^1_{(R)} G_0 t^{(R)} G_0 \mathcal{U}^{12}_{(R)}, \tag{2b}$$

for $2 + 2$ as the initial state. In both sets of equations G_0 is the four free particle Green's function and $t^{(R)}$ the $2N$ t matrix derived from nuclear potential plus screened Coulomb between pp pairs. The operators $U^\alpha_{(R)}$, obtained from

$$U^\alpha_{(R)} = P_\alpha G_0^{-1} + P_\alpha t^{(R)} G_0 U^\alpha_{(R)}, \tag{3a}$$

$$P_1 = P_{12} P_{23} + P_{13} P_{23}, \tag{3b}$$

$$P_2 = P_{13} P_{24}, \tag{3c}$$

are the symmetrized AGS operators for the $1 + (3)$ and $(2) + (2)$ subsystems and P_{ij} is the permutation operator of particles i and j. The amplitudes for all possible transitions between two-cluster states with relative two-body momenta $\mathbf{p}_i$ and $\mathbf{p}_f$

are obtained from

$$\langle \mathbf{p}_f | T^{\alpha\beta}_{(R)} | \mathbf{p}_i \rangle = S_{\alpha\beta} \langle \phi^{(R)}_\alpha(\mathbf{p}_f) | \mathcal{U}^{\alpha\beta}_{(R)} | \phi^{(R)}_\beta(\mathbf{p}_i) \rangle, \quad (4)$$

where $|\phi^{(R)}_\alpha(\mathbf{p})\rangle = G_0 t^{(R)} P_\alpha |\phi^{(R)}_\alpha(\mathbf{p})\rangle$ are the Faddeev amplitudes of the initial/final $1+(3)$ and $(2)+(2)$ states and $S_{11}=3$, $S_{21}=\sqrt{3}$, $S_{22}=2$, and $S_{12}=2\sqrt{3}$ are the weight factors resulting from the symmetrization.

In close analogy with p-d elastic scattering, the full scattering amplitude $T^{\alpha\beta}_{(R)}$ calculated between initial and final p-^{3}H or d-d states may be decomposed into the long-range part $t^{\text{c.m.}}_{\alpha R}\delta_{\alpha\beta}$ and the remaining Coulomb-distorted short-range part $[T^{\alpha\beta}_{(R)} - t^{\text{c.m.}}_{\alpha R}\delta_{\alpha\beta}]$ as demonstrated in Ref. [10]. $t^{\text{c.m.}}_{\alpha R}$ is the two-body t matrix derived from the screened Coulomb potential between the proton and the center of mass (c.m.) of ^{3}H for $\alpha = 1$ and between the c.m. of both deuterons for $\alpha = 2$. Applying the renormalization procedure, i.e., multiplying $\langle \mathbf{p}_f | T^{\alpha\beta}_{(R)} | \mathbf{p}_i \rangle$ by the renormalization factors $[Z^\alpha_R]^{-\frac{1}{2}}$ on the left and $[Z^\beta_R]^{-\frac{1}{2}}$ on the right [8,10], in the $R\to\infty$ limit, yields the full transition amplitude in the presence of Coulomb

$$\langle \mathbf{p}_f | T^{\alpha\beta} | \mathbf{p}_i \rangle = \langle \mathbf{p}_f | t^{\text{c.m.}}_{\alpha C} | \mathbf{p}_i \rangle \delta_{\alpha\beta} + \lim_{R\to\infty} \Big\{ \big[Z^\alpha_R\big]^{-\frac{1}{2}} \times \langle \mathbf{p}_f | \big[T^{\alpha\beta}_{(R)} - t^{\text{c.m.}}_{\alpha R}\delta_{\alpha\beta}\big] | \mathbf{p}_i \rangle \big[Z^\beta_R\big]^{-\frac{1}{2}} \Big\}, \quad (5)$$

where the $[Z^\alpha_R]^{-1}\langle \mathbf{p}_f | t^{\text{c.m.}}_{\alpha R} | \mathbf{p}_i \rangle$ converges (in general, as a distribution) to the exact Coulomb amplitude $\langle \mathbf{p}_f | t^{\text{c.m.}}_{\alpha C} | \mathbf{p}_i \rangle$ between the proton and the c.m. of the ^{3}H nucleus (between the c.m. of both deuterons) and therefore is replaced by it. The renormalization factor $Z^\alpha_R = \exp(-2i(\sigma^\alpha_L - \eta^\alpha_{LR}))$ is employed in the partial-wave dependent form as in Refs. [8] and [14] with the diverging screened Coulomb p-^{3}H(d-d) phase shift η^α_{LR} corresponding to standard boundary conditions and the proper Coulomb one σ^α_L referring to the logarithmically distorted proper Coulomb boundary conditions. L is the orbital angular momentum between the two clusters. Obviously, there is no long-range Coulomb force in the n-^{3}He states; in that case $\langle \mathbf{p}_f | t^{\text{c.m.}}_{\alpha C} | \mathbf{p}_i \rangle = \langle \mathbf{p}_f | t^{\text{c.m.}}_{\alpha R} | \mathbf{p}_i \rangle = 0$ and $\sigma^\alpha_L = \eta^\alpha_{LR} = 0$. The second term in Eq. (5), after renormalization by $[Z^\alpha_R]^{-\frac{1}{2}}[Z^\beta_R]^{-\frac{1}{2}}$, represents the Coulomb-modified nuclear short-range amplitude. It has to be calculated numerically, but, because of its short-range nature, the $R\to\infty$ limit is reached with sufficient accuracy at finite screening radii R as demonstrated in Refs. [8] and [14] for p-d and p-^{3}He scattering. As found there, one needs larger values of R at lower energies, making the convergence of the results more difficult to reach. Nevertheless, for $E_p > 1$ MeV or $E_d > 1$ MeV the method leads to very precise results. Depending on the reaction and the energy, we obtain fully converged results for n-^{3}He, p-^{3}H, and d-d observables with R ranging from 10 to 20 fm.

The results are also fully converged with respect to the partial-wave expansion. The calculations include isospin-singlet $2N$ partial waves with total angular momentum $I \leqslant 4$ and isospin-triplet $2N$ partial waves with orbital angular momentum $l_x \leqslant 6$, $3N$ partial waves with spectator orbital angular momentum $l_y \leqslant 6$ and total angular momentum $J \leqslant \frac{13}{2}$, $4N$ partial waves with $1+3$ and $2+2$ orbital angular momentum $l_z \leqslant 6$, resulting in up to about 15 000 channels for fixed $4N$ total angular momentum and parity. Initial/final two-cluster states with relative orbital angular momentum $L \leqslant 5$ are included for the calculation of observables. For some reactions, e.g., n-^{3}He elastic scattering, the partial-wave convergence is considerably faster, allowing for a reduction in the employed angular momentum cutoffs.

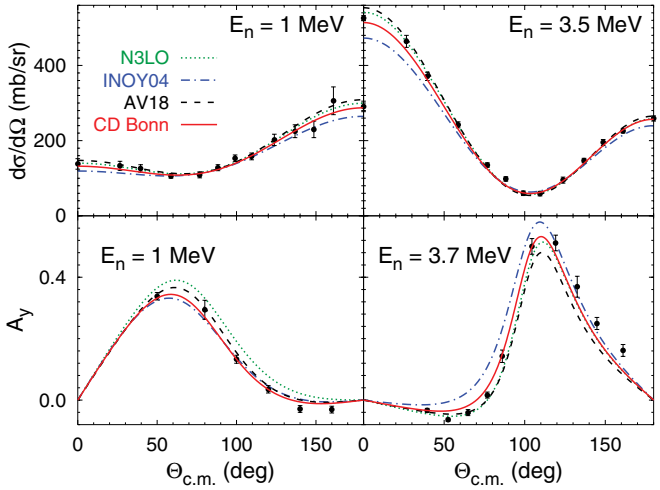

FIG. 1. (Color online) Differential cross section and neutron analyzing power of elastic n-^{3}He scattering at 1, 3.5, and 3.7 MeV neutron laboratory energy. Results obtained with potentials CD Bonn (solid curves), AV18 (dashed curves), INOY04 (dashed-dotted curves), and N3LO (dotted curves) are compared. The cross section data are from Ref. [21], and A_y data are from Ref. [22] at 1 MeV and from Ref. [23] at 3.7 MeV.

The two-nucleon interactions we use are charge-dependent Bonn (CD Bonn) [17], AV18 [18], the inside nonlocal outside Yukawa (INOY04) potential by Doleschall [19], and the one derived from chiral perturbation theory at next-to-next-to-next-to-leading order (N3LO) [20]. Although we do not include a $3N$ force, its presence is simulated by using the potential INOY04 that fits both ^{3}He and ^{3}H experimental binding energies (7.72 MeV and 8.48 MeV, respectively). In Figs. 1 through 5 we show the results for six different reactions. The most remarkable findings are the following: (a) the excellent agreement with the data for the calculated d-d elastic differential cross section in Fig. 3; (b) the lack of a large A_y deficiency in n-^{3}He and p-^{3}H (see Figs. 1 and 2) unlike what was observed before in p-^{3}He [14,16]; and

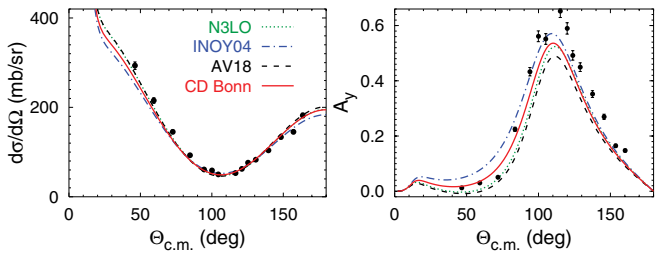

FIG. 2. (Color online) Differential cross section and proton analyzing power of elastic p-^{3}H scattering at 4.15 MeV proton laboratory energy. Curves are as described in legend to Fig. 1. The data are from Ref. [24].

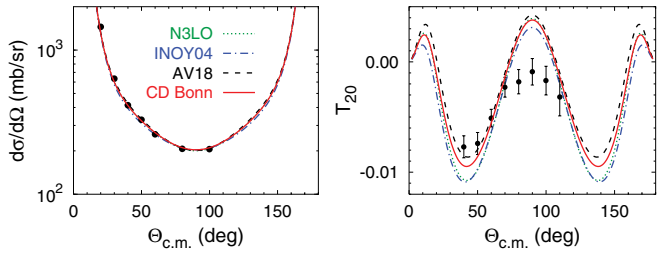

FIG. 3. (Color online) Differential cross section and deuteron tensor analyzing power T_{20} of elastic d-d scattering at 3 MeV deuteron laboratory energy. Curves are as described in legend to Fig. 1. The cross section data are from Ref. [25] and T_{20} data are from Ref. [26].

(c) the overall description of $d + d \rightarrow n + {}^3\mathrm{He}$ and $d + d \rightarrow p + {}^3\mathrm{H}$ data presented in Fig. 5, given its complex structure.

Of all the potentials we use, only INOY04 represents both n-^{3}He and p-^{3}H thresholds in the correct position. For this reason it is perhaps not surprising to see that this potential gives rise to the best description of $d + d \rightarrow n + {}^3\mathrm{He}$ and $d + d \rightarrow p + {}^3\mathrm{H}$ data, including the differential cross section. Nevertheless, even if the correct position of thresholds is an important factor, it is certainly not the only one that matters because in n-^{3}He elastic scattering (Fig. 1) and $p + {}^3\mathrm{H} \rightarrow n + {}^3\mathrm{He}$ (Fig. 4) INOY04 gives rise to results that are poorer than those obtained with other potentials.

The largest disagreements with the data are observed in a very small d-d elastic T_{20} at 90° shown in Fig. 3 and in the $p + {}^3\mathrm{H} \rightarrow n + {}^3\mathrm{He}$ proton analyzing power and differential cross section at forward and backward angles at low energies in Fig. 4. At $E_p = 2.48$ MeV we find two sets of data that are inconsistent at backward angles but where this work does not help to resolve given the wide range of results obtained with the potentials we use. At $E_p = 6$ MeV the results in Fig. 4 are almost independent of the choice of potentials but they all

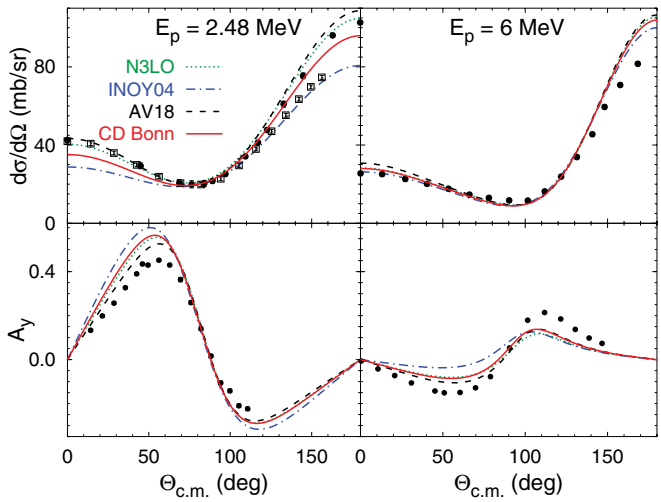

FIG. 4. (Color online) Differential cross section and proton analyzing power of $p + {}^3\mathrm{H} \rightarrow n + {}^3\mathrm{He}$ reaction at 2.48 and 6 MeV proton laboratory energy. Curves are as described in legend to Fig. 1. The cross section data are from Refs. [27] (circles) and [28] (squares) at 2.48 MeV and from Ref. [29] at 6 MeV. A_y data are from Ref. [30] at 2.48 MeV and from Ref. [31] at 6 MeV.

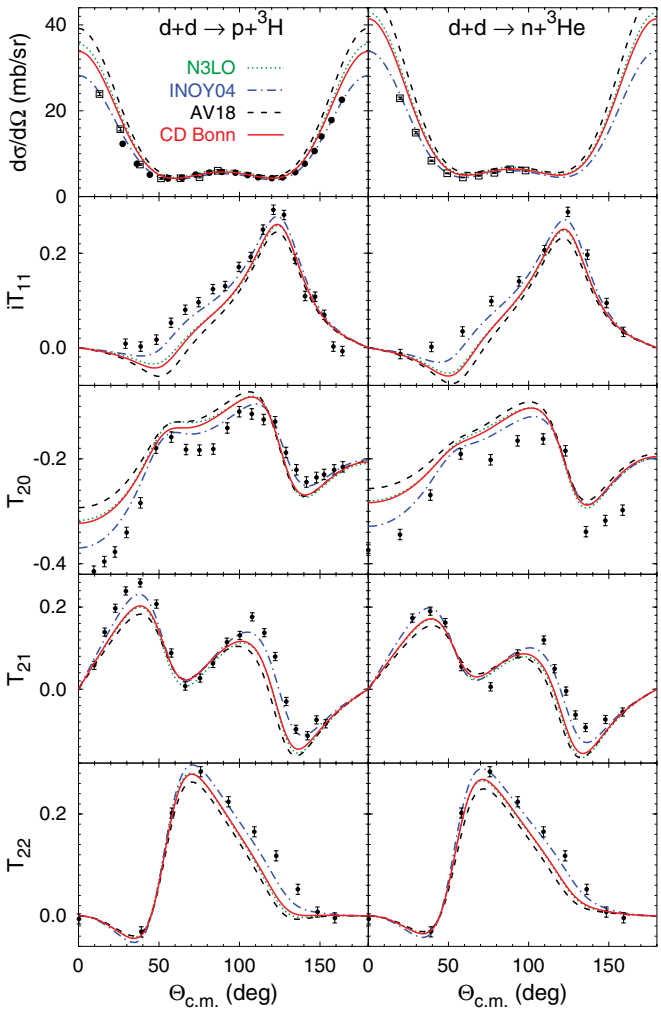

FIG. 5. (Color online) Differential cross section and deuteron analyzing powers of $d + d \rightarrow p + {}^3\mathrm{H}$ and $d + d \rightarrow n + {}^3\mathrm{He}$ reactions at 3 MeV deuteron laboratory energy. Curves are as described in legend to Fig. 1. The cross section data are from Refs. [32] (squares) and [33] (circles). Analyzing power data are from Ref. [33] for $d + d \rightarrow p + {}^3\mathrm{H}$ and from Ref. [34] for $d + d \rightarrow n + {}^3\mathrm{He}$.

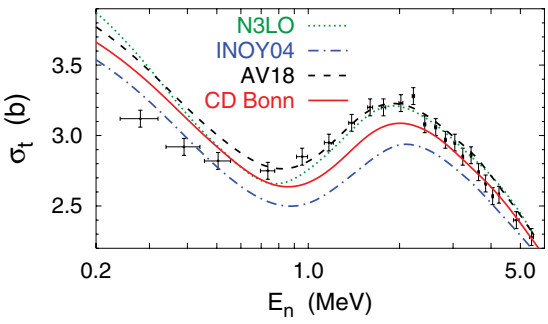

FIG. 6. (Color online) n-^{3}He total cross section as function of the neutron laboratory energy. Curves are as described in legend to Fig. 1. The data are from Ref. [35].

miss the data at backward angles. The problems in n-^{3}He and p-^{3}H reactions may be associated with the 0^+ excited state of the α particle that sits between the two thresholds and whose position changes with the potential we choose.

Finally in Fig. 6 we show the total n-^{3}He cross section as a function of energy. Again we find an agreement with data that, depending on the potential, is either similar (INOY04) or better (N3LO and AV18) than observed in n-^{3}H [13]. As in the n-^{3}H total cross section [13], the curves pertaining to AV18 and N3LO calculations exchange position at about the same excitation energy relative to the n-^{3}H threshold ($E \simeq 1.3$ MeV) but now N3LO leads to the highest total cross section at low energy instead of at the resonance peak. The reason for this behavior may reside in the relative position of the 0^- ($^3P_0$) inelastic resonance [36] that is associated with the 0^- $\mathcal{T} = 0$ state at about 0.4 MeV excitation above the n-^{3}He threshold.

In conclusion, we show for the first time results of *ab initio* calculations involving four-nucleon reactions initiated by either n-^{3}He, p-^{3}H, and d-d. Realistic nuclear potentials are used between hadron pairs plus the Coulomb interaction between protons. Although specific observables show discrepancies with data that need further investigation, namely, the inclusion of three-nucleon forces, the results give a reasonable overall description of the data for all six reactions that show an improvement relative to what is found for $\mathcal{T} = 1$ observables [13,14]. Work is in progress to study the effect of three-nucleon forces through the inclusion of Δ degrees of freedom.

The authors thank W. Grüebler for providing experimental data. A.D. is supported by Fundação para a Ciência e a Tecnologia (FCT) Grant SFRH/BPD/14801/2003 and A.C.F. is supported in part by FCT Grant POCTI/ISFL/2/275.

[1] S. C. Pieper, V. R. Pandharipande, R. B. Wiringa, and J. Carlson, Phys. Rev. C **64**, 014001 (2001).
[2] S. C. Pieper, K. Varga, and R. B. Wiringa, Phys. Rev. C **66**, 044310 (2002).
[3] E. Caurier, P. Navratil, W. E. Ormand, and J. P. Vary, Phys. Rev. C **66**, 024314 (2002).
[4] W. Glöckle *et al*., Phys. Rep. **274**, 107 (1996).
[5] A. Kievsky, M. Viviani, and S. Rosati, Phys. Rev. C **64**, 024002 (2001).
[6] R. Lazauskas and J. Carbonell, Phys. Rev. C **70**, 044002 (2004); R. Lazauskas *et al*., *ibid*. **71**, 034004 (2005).
[7] M. Viviani, A. Kievsky, S. Rosati, E. A. George, and L. D. Knutson, Phys. Rev. Lett. **86**, 3739 (2001).
[8] A. Deltuva, A. C. Fonseca, and P. U. Sauer, Phys. Rev. C **71**, 054005 (2005); **72**, 054004 (2005); Phys. Rev. Lett. **95**, 092301 (2005).
[9] J. R. Taylor, Nuovo Cimento B **23**, 313 (1974); M. D. Semon and J. R. Taylor, Nuovo Cimento A **26**, 48 (1975).
[10] E. O. Alt and W. Sandhas, Phys. Rev. C **21**, 1733 (1980).
[11] K. M. Nollett *et al*., arXiv:nucl-th/0612035.
[12] P. Grassberger and W. Sandhas, Nucl. Phys. **B2**, 181 (1967); E. O. Alt, P. Grassberger, and W. Sandhas, JINR Report No. E4-6688, 1972.
[13] A. Deltuva and A. C. Fonseca, Phys. Rev. C **75**, 014005 (2007).
[14] A. Deltuva and A. C. Fonseca, Phys. Rev. Lett. **98**, 162502 (2007).
[15] A. C. Fonseca, Phys. Rev. Lett. **83**, 4021 (1999).
[16] B. M. Fisher *et al*., Phys. Rev. C **74**, 034001 (2006).
[17] R. Machleidt, Phys. Rev. C **63**, 024001 (2001).
[18] R. B. Wiringa, V. G. J. Stoks, and R. Schiavilla, Phys. Rev. C **51**, 38 (1995).
[19] P. Doleschall, Phys. Rev. C **69**, 054001 (2004).
[20] D. R. Entem and R. Machleidt, Phys. Rev. C **68**, 041001(R) (2003).
[21] J. D. Seagrave, L. Cranberg, and J. E. Simmons, Phys. Rev. **119**, 1981 (1960).
[22] P. Jany *et al*., Nucl. Phys. **A483**, 269 (1988).
[23] H. O. Klages *et al*., Nucl. Phys. **A443**, 237 (1985).
[24] R. Kankowsky *et al*., Nucl. Phys. **A263**, 29 (1976).
[25] J. M. Blair *et al*., Phys. Rev. **74**, 1594 (1948).
[26] B. J. Crowe *et al*., Phys. Rev. C **61**, 034006 (2000).
[27] M. Drosg, Nucl. Sci. Eng. **67**, 190 (1978).
[28] G. A. Jarvis, Los Alamos Scientific Lab Report No. 2014, 1956, p. 35.
[29] W. E. Wilson, R. L. Walter, and D. B. Fossan, Nucl. Phys. **27**, 421 (1961).
[30] M. A. Doyle *et al*., Nucl. Phys. **A371**, 225 (1981).
[31] J. J. Jarmer *et al*., Phys. Rev. C **9**, 1292 (1974).
[32] J. M. Blair *et al*., Phys. Rev. **74**, 1599 (1948).
[33] W. Grüebler *et al*., Nucl. Phys. **A193**, 129 (1972).
[34] L. J. Dries *et al*., Phys. Lett. **B80**, 176 (1979).
[35] Los Alamos Physics and Cryogenics Group, Nucl. Phys. **12**, 291 (1959).
[36] A. C. Fonseca *et al*., Few-Body Syst. **31**, 139 (2002).